ARTICLES
PUBLISHED ONLINE: 23 NOVEMBER 2015 | DOI: 10.1038/NNANO.2015.256
nature nanotechnology

Reversible trapping and reaction acceleration within dynamically self-assembling nanoflasks

Hui Zhao[1], Soumyo Sen[2], T. Udayabhaskararao[1], Michał Sawczyk[1], Kristina Kučanda[1], Debasish Manna[1], Pintu K. Kundu[1], Ji-Woong Lee[1], Petr Král[2,3,4] and Rafal Klajn[1]*

The chemical behaviour of molecules can be significantly modified by confinement to volumes comparable to the dimensions of the molecules. Although such confined spaces can be found in various nanostructured materials, such as zeolites, nanoporous organic frameworks and colloidal nanocrystal assemblies, the slow diffusion of molecules in and out of these materials has greatly hampered studying the effect of confinement on their physicochemical properties. Here, we show that this diffusion limitation can be overcome by reversibly creating and destroying confined environments by means of ultraviolet and visible light irradiation. We use colloidal nanocrystals functionalized with light-responsive ligands that readily self-assemble and trap various molecules from the surrounding bulk solution. Once trapped, these molecules can undergo chemical reactions with increased rates and with stereoselectivities significantly different from those in bulk solution. Illumination with visible light disassembles these nanoflasks, releasing the product in solution and thereby establishes a catalytic cycle. These dynamic nanoflasks can be useful for studying chemical reactivities in confined environments and for synthesizing molecules that are otherwise hard to achieve in bulk solution.

Nature has long-inspired chemists with its ability to stabilize ephemeral chemical species[1], perform chemical reactions at unprecedented rates[2,3] and selectivities[4], and synthesize complex molecules[5,6] and inorganic nanostructures[7,8] with seemingly effortless ease. However, chemists and natural systems perform reactions in fundamentally different ways: whereas chemists typically carry out reactions between molecules moving around freely in solution, natural systems consistently use the effect of nanoscale confinement. Several creative approaches have been devised to mimic the confined spaces engineered by nature and to investigate the behaviour of small-molecule guests within them. For example, assembling molecules on nucleic acid templates can drastically increase their effective molarities and consequently the rate of chemical reactions between them[9,10]. Considerable attention has been devoted to molecular and supramolecular hosts—entities capable of binding smaller molecules in their cavities. Here, notable examples of reactivity modulation include the stabilization of both white phosphorus[11] and cyclic trimers of siloxanes[12], as well as the induction of unusual regioselectivities in the Diels–Alder reaction[13]. The behaviour of chemical species within the confinement of zeolites[14,15] and other nanoporous materials[16,17], emulsion microdroplets[18], hydrogels[19], lipidic cubic phases[20] and coacervate droplets[21] has also been studied. In contrast, the properties of molecular guests within confined spaces (nanosized pores) between inorganic nanoparticles self-assembled into colloidal crystals[22–26] have been explored only to a limited extent, probably because of the slow diffusion of molecules to and from these 'nanoflasks'. Here, we have overcome this diffusion limitation by creating such colloidal crystals in a reversible fashion using light at two different wavelengths.

Reversible control of nanoflask formation using light

As the precursors of our nanoflasks, we used azobenzene-functionalized inorganic nanoparticles of different sizes and compositions, including 6 nm gold[27,28], 11 nm magnetite[29,30] and 17 nm silica particles (Fig. 1a and Supplementary Sections 1–6). Depending on the composition of the particle core, we used different binding groups to immobilize the azobenzene moiety: thiols for Au, catechols for Fe_3O_4 and silanes for SiO_2 (ligands **1**, **2** and **3**, respectively, in Fig. 1b). Solutions of these azobenzene-decorated nanoparticles in nonpolar solvents (here, toluene) were stable for at least several months under ambient light conditions. In contrast, when exposed to ultraviolet light (365 nm, 0.7 mW cm^{-2}), the nanoparticles self-assembled (within minutes) as a result of loss of the solvation layer[31] (owing to poor solvation of the polar *cis*-azobenzenes by toluene) and the emergence of attractive dipole–dipole interactions between *cis*-azobenzene moieties on different nanoparticles[32]. The product of the self-assembly process depended on the overall volume fraction, χ, of the nanoparticles: for $\chi < 10^{-4}$ vol/vol, the aggregates were relatively small (less than $\sim 3 \times 10^5$ particles) and amorphous, whereas at higher concentrations, we observed the formation of well-defined crystalline aggregates. Within these supracrystals, the nanoparticles were closely packed, giving rise to cavities, each surrounded by four particles arranged in a tetrahedral geometry (Fig. 1c).

Reversible trapping within self-assembling nanoflasks

The essentially polar (*cis*-azobenzene-rich) nature of the cavities is not ideal for hosting the nonpolar toluene molecules, which, like high-energy water molecules inside the cavities of selected molecular containers[33–36], could readily be displaced by a wide range of more suitable guest molecules. Consequently, we presumed that polar additives (blue spheres in Fig. 1d) present in the solution during the self-assembly process would be trapped inside these cavities much more readily than the toluene molecules (red spheres). Experiments in which we attempted to self-assemble 6 nm Au·**1** ($c = 0.363$ μM) in the presence of increasing volume fractions of (polar) methanol corroborated this reasoning. These experiments showed that the rate of nanoparticle self-assembly was inversely

[1]Department of Organic Chemistry, Weizmann Institute of Science, Rehovot 76100, Israel. [2]Department of Chemistry, University of Illinois at Chicago, Chicago, Illinois 60607, USA. [3]Department of Physics, University of Illinois at Chicago, Chicago, Illinois 60607, USA. [4]Department of Biopharmaceutical Sciences, University of Illinois at Chicago, Chicago, Illinois 60607, USA. *e-mail: rafal.klajn@weizmann.ac.il

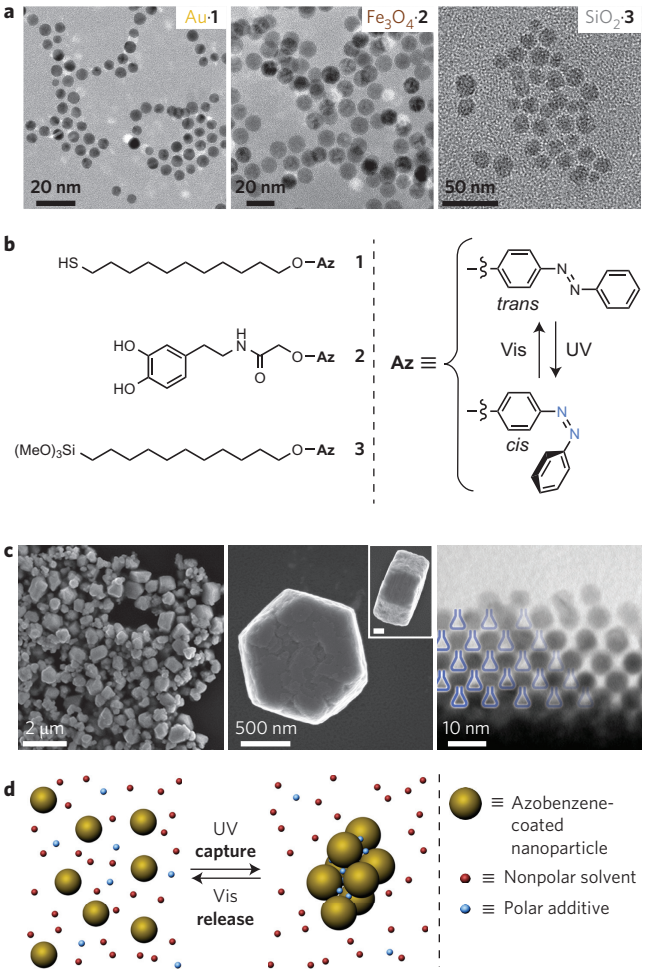

Figure 1 | Reversible self-assembly of azobenzene-functionalized nanoparticles and nanoflasks formation. a, Transmission electron microscopy (TEM) images of (left to right) photoresponsive 6 nm Au, 11 nm Fe_3O_4 and 17 nm SiO_2 nanoparticles used to generate dynamically self-assembling nanoflasks. **b**, Structural formulae of ligands **1**–**3** used for preparing photoresponsive Au, Fe_3O_4 and SiO_2 nanoparticles (left) and light-controlled azobenzene isomerization (right). The *cis* isomer of azobenzene induces self-assembly of nanoparticles. **c**, Electron micrographs (at different magnifications) of colloidal crystals prepared by exposing 6 nm Au·**1** to ultraviolet light (scale bar in the inset, 200 nm). **d**, Schematic representation of the reversible trapping of polar molecules during light-induced self-assembly of photoresponsive nanoparticles. Az, azobenzene; UV, ultraviolet light; Vis, visible light.

proportional to the amount of methanol, and no aggregation whatsoever was observed in solutions containing 4% vol/vol (or more) methanol, most likely because of the stabilization of *cis*-azobenzenes by the methanol (Supplementary Section 7). Based on these observations, it is reasonable to assume that nanoparticle aggregates obtained in the presence of $0 < x < 4\%$ of methanol trap the polar solvent molecules in their cavities.

A dramatic manifestation of the trapping process is shown in Fig. 2a. In this experiment, 6 nm Au·**1** nanoparticles were assembled in technical-grade toluene (containing residual water) and the resulting aggregates were deposited on a carbon-coated copper transmission electron microscope (TEM) grid in the dark (to avoid visible light-induced disassembly). Following prolonged (~30 s) exposure to a focused electron beam during TEM imaging, these aggregates rapidly disintegrated ('exploded'), with some nanoparticles expelled to distances equivalent to more than ten times the diameter of the aggregate they originally comprised (Fig. 2a, right, and Supplementary Section 8). We observed analogous results with dry (distilled) toluene to which we intentionally added trace amounts of water. Notably, however, no such explosions occurred when dry toluene was used, with aggregates remaining unaffected even after several minutes of exposure to the electron beam. These results can be explained by the local heating induced by the electron beam facilitating back-isomerization of the metastable *cis* to *trans* configuration of azobenzene (Fig. 1b). The trapped water molecules tend to avoid the resulting hydrophobic (*trans*-azobenzene-rich) environment, causing an explosion under the low (3×10^{-7} mbar) pressures typical for operating the TEM. Experiments in which visible light was used to irradiate the aggregates deposited on the TEM grids before inspecting the sample by TEM confirmed this explanation; here, the aggregates exploded solely as a result of the reduced pressure (without prolonged exposure to a focused electron beam).

To better understand the mechanism underlying this trapping and release of water (and therefore other polar guest molecules), we studied the affinity of water to *trans*- and *cis*-azobenzene-functionalized nanoparticles by atomistic molecular dynamics (MD) simulations (Supplementary Section 9). We first considered three 2.6 nm Au·**1** in a $21.5 \times 18.5 \times 10$ nm^3 box of toluene permanently saturated with water. We found that only *cis*-**1**-coated nanoparticles spontaneously assembled, in agreement with the experimental observations. Upon assembly, each of the *cis*-**1**-coated nanoparticles captured, on average, five to seven water molecules, which interacted with the particles by hydrogen bonding to the azobenzene nitrogen atoms (Fig. 2b, right). In contrast, *trans*-**1**-decorated nanoparticles remained separated and had no appreciable affinity to water molecules (Fig. 2c). In addition, we investigated the stability of water clusters inside the cavities formed by four *cis*-**1**-coated particles arranged in a tetrahedral configuration and found that clusters comprising ≥10 water molecules were highly stable (Supplementary Fig. 26a; in comparison, a cluster of ten water molecules in pure toluene rapidly disintegrated). This suggests a possible role of the nanoparticles (specifically, electric fields generated by the *cis*-azobenzene moieties) in promoting attractive interactions between polar molecules. Visible light-induced disassembly of nanoparticle aggregates induced a rapid release of water (Supplementary Fig. 27), in agreement with experimental observations.

Quantifying and visualizing the trapping process

Next, we attempted to quantify the number of polar molecules trapped inside the cavities. We worked with a model compound exhibiting strong absorption in the visible region, namely, a nitrobenzoxadiazole (NBD)-based dye, modified with the polar OH group (**4** in Fig. 3a; also Supplementary Section 10). Once the nanoparticles were assembled in toluene in the presence of the dye, we could easily separate them from the supernatant by centrifugation, and the amount of trapped **4** was quantified spectrophotometrically. The amount of **4** captured by 6 nm Au·**1** nanoparticles increased with an increasing dye-to-particle molar ratio (Fig. 3a); however, it never exceeded 26 molecules per particle, even for very high (for example, 1,000) ratios; that is, non-trapped molecules remained dissolved in the solution. Interestingly, when much smaller, 2.6 nm Au·**1** nanoparticles were used instead, the aggregates contained no detectable amount of **4** (presumably because the entropy of trapped molecules is too low in the cavities between very small nanoparticles). From these experiments we can conclude that the trapping ability strongly depends on the nanoparticle size (that is, on the dimensions of the nanoflasks that are formed when the nanoparticles self-assemble), with nanoflasks derived from particles of a given size being able to trap only a specific number of guest molecules.

To determine the generality of our method and to further confirm that trapping is facilitated by the formation of hydrogen

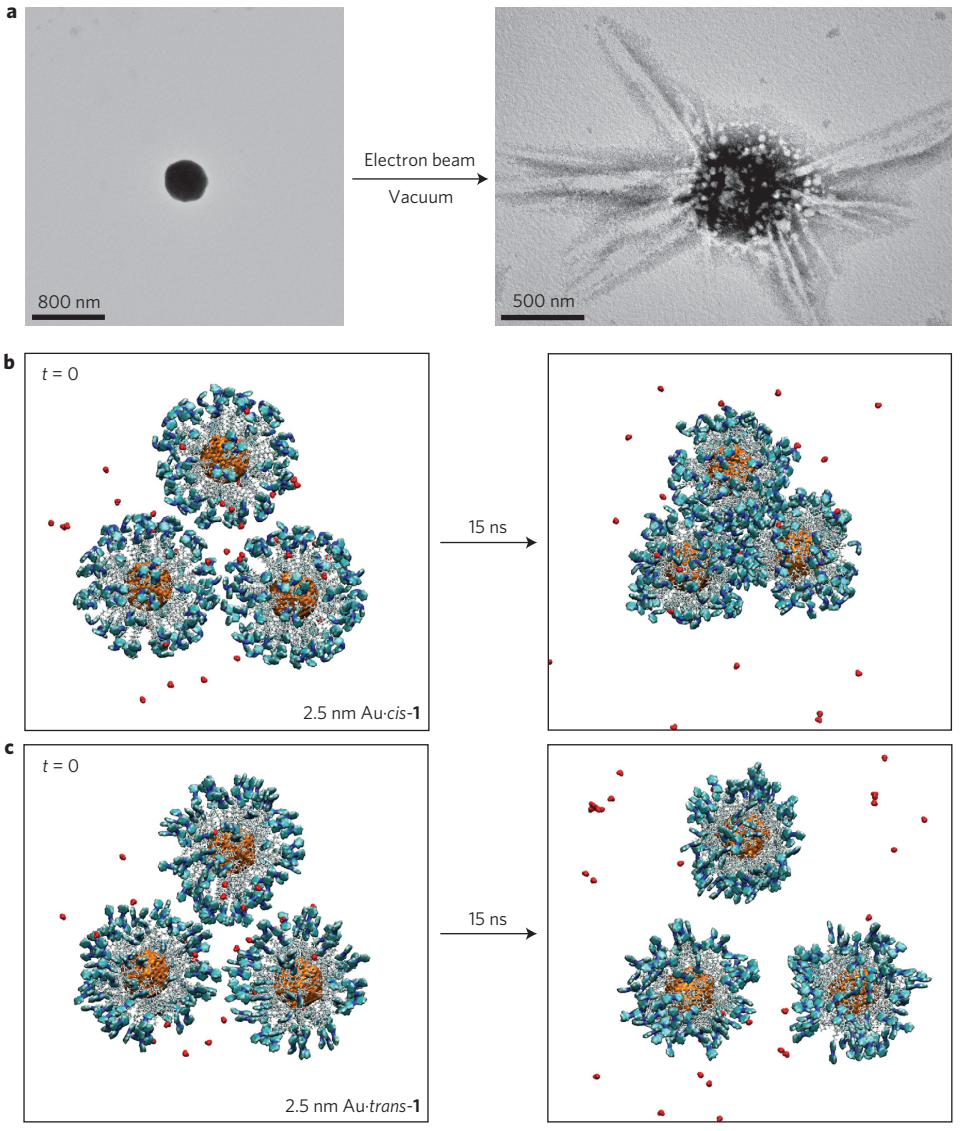

Figure 2 | Trapping of water within self-assembling nanoflasks. a, Left: TEM image of an individual aggregate of 6 nm Au·**1** nanoparticles prepared by irradiating Au·**1** nanoparticles with ultraviolet light in toluene in the presence of a small amount of water and deposited on the TEM substrate in the dark. Right: on exposing the Au·**1** nanoparticle aggregate to a focused electron beam for ~30 s, *cis*-azobenzene undergoes back-isomerization to the *trans* form, which causes the release of the trapped water molecules and a rapid 'explosion' of the aggregate. **b**,**c**, Snapshots from atomistic simulations of *cis*-**1**-functionalized and *trans*-**1**-functionalized 2.6 nm Au nanoparticles in toluene saturated with water (shown in red; toluene molecules omitted for clarity). Only in the case of *cis*-azobenzene nanoparticle aggregation and trapping of water is observed.

bonds between the guest molecules and the nanoparticle-bound *cis*-azobenzene moieties, we studied the trapping of model compounds containing various functional groups (Supplementary Section 11). We found that the self-assembling nanoparticles strongly favoured the trapping of molecules that can act as hydrogen-bond donors (for example, alcohols, primary amines). Compounds featuring only hydrogen-bond acceptor sites (for example, tertiary amines, ethers and ketones) were not trapped. Interestingly, in the course of these studies we found that molecules featuring extended aromatic systems (for example, anthracene, pyrene) are also readily trapped even in the absence of hydrogen-bond donors. This result can be rationalized by the formation of π–π stacking interactions between the azobenzene groups and the aromatic guests. Each of the trapped compounds could be released during visible light-induced disassembly of nanoparticle aggregates. One limitation of our methodology is the possibility of the ligand-exchange reaction occurring between the trapped guests and the thiols originally bound to the nanoparticle surfaces—for example, dodecanethiol used as a potential guest gradually displaced **1** from the surfaces of 6 nm Au·**1**. Nevertheless, thiols could be reversibly trapped with other types of photoswitchable nanoparticles (for example, Fe_3O_4·**2** and SiO_2·**3**).

It was also of interest to determine the selectivity of trapping when working with more than one type of potential guest. We therefore studied model mixtures of a nonpolar alkyne **5** with more polar hydroxyalkynes **6** and **7** (Fig. 3a; also Supplementary Section 12). In each experiment, an equimolar mixture of alkynes (**5** + **6** or **5** + **7**) was exposed to the self-assembling nanoparticles (6 nm Au·**1**) and the resulting aggregates were then collected and analysed in terms of the **6**:**5** or **7**:**5** ratio. In all cases the nanoparticles captured the hydroxyalkynes in preference to **5**, with **7** (which lacks a hydrophobic 2-pentyl substituent of **6**) achieving higher occluded concentrations than **6**. The selectivity of trapping increased as the alkyne-to-nanoparticle ratio decreased, such that the **7**:**5** ratio could be increased by as many as 100 times in a single trapping event (Fig. 3b, black data points).

In an effort to directly visualize the trapping of polar species with azobenzene-coated nanoparticles, we worked with mixtures of 17 nm

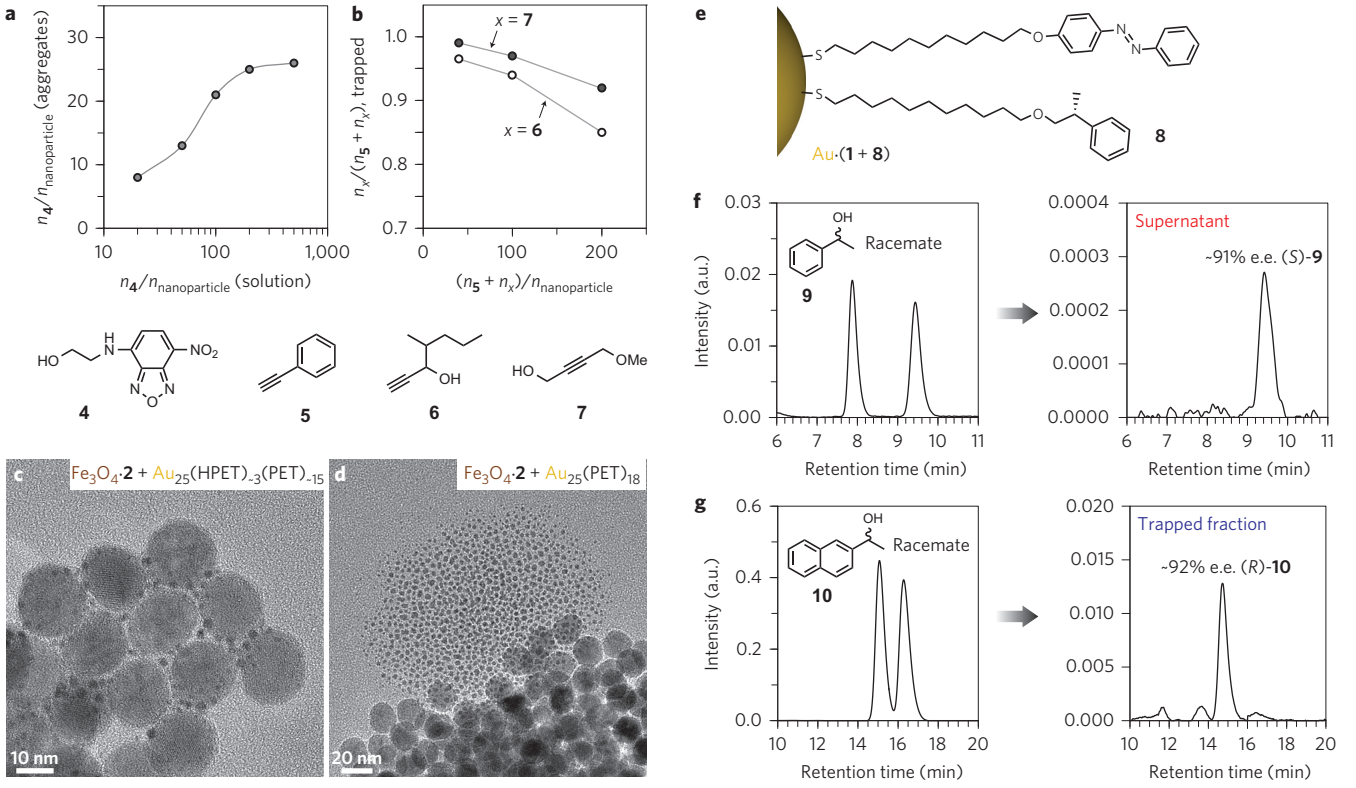

Figure 3 | Quantifying and visualizing the trapping process. a, Efficiency with which 6 nm Au·**1** nanoparticles trap dye **4** (*y* axis: molar ratio of **4** to nanoparticles in the aggregates) as a function of the molar ratio of **4**-to-Au·**1** in solution (*x* axis). Even for very high **4**-to-Au·**1** ratios in solution, only up to ~26 molecules per nanoparticle are trapped. **b**, Trapping selectivity for polar alkynes **6** or **7** in the presence of nonpolar **5**. The experiments were performed by assembling 6 nm Au·**1** nanoparticles in the presence of equimolar amounts of the two alkynes, removing the aggregated particles and quantifying the alkynes remaining in the supernatant. A *y* value of 0.5 corresponds to equal trapping efficiency for the two alkynes. The symbol 'x' refers to alkynes **6** or **7**. **c**, Direct visualization of the trapping process. Here, polar Au_{25} nanoclusters co-functionalized with 2-(4-hydroxyphenyl)ethanethiol (HPET) and 2-phenylethanethiol (PET) were trapped by 17 nm Fe_3O_4·**2** nanoparticles by exposing a 100:1 mixture of nanoclusters and nanoparticles to ultraviolet light. **d**, In contrast, hydrophobic $Au_{25}(PET)_{18}$ nanoclusters are not trapped by Fe_3O_4·**2** under the same conditions (note that the majority of Au particles seen in the TEM images are larger than Au_{25} nanoclusters because of the rapid coalescence of Au_{25} under a focused electron beam). **e**, Schematic representation of a nanoparticle co-functionalized with photoresponsive and chiral ligands (**1** and **8**, respectively). **f**, Enantioselective light-induced trapping: high-performance liquid chromatography (HPLC) traces of a racemic mixture of (*R*)- and (*S*)-1-phenylethanol **9** before the trapping experiment (left, racemic) and of a supernatant after trapping and removal of the nanoparticles (right). **g**, HPLC traces of a mixture of (*R*)- and (*S*)-1-(2-naphthyl)ethanol **10** before trapping (left, racemic) and of a fraction trapped within nanoflasks (right).

Fe_3O_4·**2** and Au_{25} nanoclusters[37,38] protected with monolayers containing a polar ligand, 2-(4-hydroxy)-phenylethanethiol (HPET) (in addition to the hydrophobic 2-phenylethanethiol (PET)) (average composition, $Au_{25}(HPET)_{\sim3}(PET)_{\sim15}$; Supplementary Section 13). Specifically, a toluene solution containing approximately 100 Au nanoclusters for each Fe_3O_4 particle was exposed to 10 min of ultraviolet light and a sample for TEM was collected. As shown in Fig. 3c, the azobenzene-functionalized Fe_3O_4·**2** nanoparticles readily trapped these nanoclusters, which preferentially filled the cavities between the Fe_3O_4·**2** particles rather than simply attaching to their outer surfaces, again emphasizing the critical role of confinement in the binding process. In sharp contrast, control experiments with mixtures of 17 nm Fe_3O_4·**2** nanoparticles and the nonpolar $Au_{25}(PET)_{18}$ (100 nanoclusters for each particle) revealed no trapping of nanoclusters—these nanoclusters formed separate islands on the TEM substrates (Fig. 3d).

Enantioselective trapping within chiral nanoflasks

An advantage of nanoparticles as precursors of confined environments is the possibility to functionalize their surfaces with more than one type of functional ligand. Having the 'interior walls' of nanoflasks decorated with desired molecules might increase the trapping selectivity towards selected molecules in the surrounding solution. To verify this hypothesis, we prepared 6 nm Au nanoparticles co-functionalized with a 1:1 mixture of azobenzene **1** and a chiral thiol **8** (Au·(**1**+**8**) in Fig. 3e; also Supplementary Section 14). The presence of non-photoresponsive ligand **8** did not affect the behaviour of these particles, which self-assembled upon exposure to ultraviolet to yield colloidal crystals incorporating chiral nanoflasks. In the proof-of-concept experiments, we attempted to enantioselectively trap chiral alcohols **9** and **10** (Fig. 3f,g). On assembling and removing Au·(**1**+**8**) from a solution containing a racemic mixture of (*R*)- and (*S*)-**9**, we found that the supernatant comprised an enantioenriched solution of **9**, with as much as ~91% enantiomeric excess (e.e.) of the (*S*) isomer. We also analysed the composition of the trapped fraction; here, we worked with a racemic mixture of (*R*)- and (*S*)-**10**, and found a considerable (~92%) excess of the (*R*) isomer within the nanoparticle aggregates (Fig. 3g and Supplementary Section 14). We hypothesize that the high level of enantioenrichment achieved in what appears to be a single enantiodiscrimination step is enabled by the dynamic nature of the self-assembly process.

Accelerating chemical reactions with dynamic nanoflasks

Next, we considered the use of nanopores within our colloidal crystals as nanoflasks for promoting chemical reactions (Fig. 4). We speculated that the increased effective molarity and/or pre-organization arising

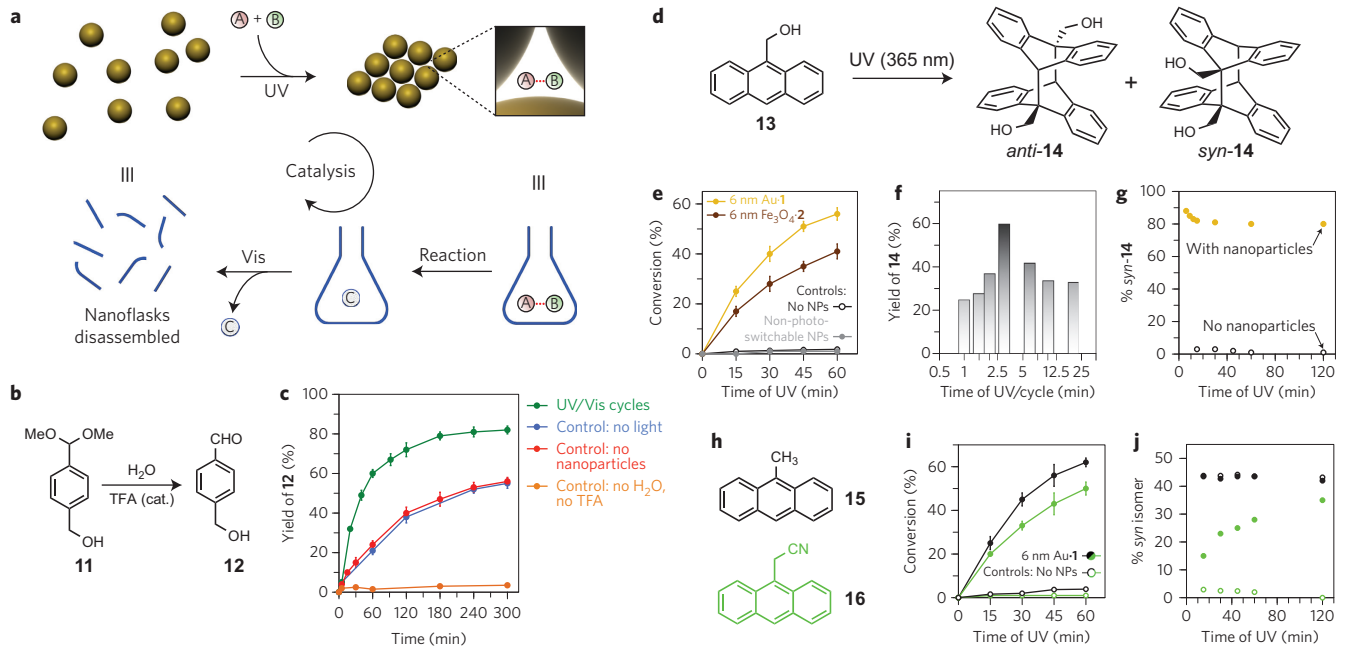

Figure 4 | Accelerating chemical reactions in dynamically self-assembling nanoflasks. a, Schematic representation of how the reversible formation of confined spaces can accelerate a chemical reaction. **b**, Reaction promotion, example I: hydrolysis of acetal **11**. **c**, Light-accelerated hydrolysis of **11**. Each cycle corresponded to irradiation for 3 min with ultraviolet light, followed by 1 min irradiation with visible light. **d**, Reaction promotion, example II: ultraviolet-induced dimerization of anthracene **13**. **e**, Light-accelerated dimerization of **13**. Each cycle corresponds to irradiation for 3 min with ultraviolet, followed by 1 min with visible light. **f**, Effect of the length of ultraviolet exposure per cycle on the conversion of **13** to its dimers. **g**, Stereoselectivity in the dimerization of **13** with and without photoswitchable nanoparticles. The composition of isomers was determined from NMR data (Supplementary Section 15). **h**, Structural formulae of additional anthracenes **15** and **16**, the reactivity of which was studied. **i**, Light-accelerated dimerization of **15** and **16**. **j**, Stereoselectivity in the dimerization of **15** and **16** with and without photoswitchable nanoparticles. NPs, nanoparticles. UV, ultraviolet.

from simultaneously trapping pairs of molecules that can potentially react with each other ('A' and 'B' in Fig. 4a) could accelerate a reaction between them. Once a product ('C' in Fig. 4a) has formed, the nanoflasks can conveniently be disintegrated by visible light and the cycle can be repeated. To verify the feasibility of this idea, we studied the acid-catalysed hydrolysis of acetal **11** to aldehyde **12** in water-saturated toluene (Fig. 4b) in the presence of 6 nm Au·**1** nanoparticles by exposing the reaction mixture to cycles of 3 min of ultraviolet and 1 min of visible light irradiation (for details see Supplementary Section 15). The reaction proceeded several times faster (green trace in Fig. 4c) than in the absence of nanoparticles (red trace), or in the presence of nanoparticles in the dark (blue trace). The relatively small acceleration was due to the high absolute concentration of **11** ($c_{\mathbf{11}} = 5$ mM). To observe a larger effect, we performed another model reaction, namely, an ultraviolet-induced anthracene (**13**) dimerization reaction[39–41] in a deoxygenated solution, at $c_{\mathbf{13}} = 10$ μM (Fig. 4d). In this case, the presence of reversibly self-assembling Au nanoparticles accelerated the dimerization of **13** by up to two orders of magnitude (yellow traces in Fig. 4e). To examine the possible role of plasmonic heating[42–44] near the Au particle surface in reaction kinetics, we performed the same reaction in the presence of self-assembling 6 nm Fe_3O_4·**2** nanoparticles (Fig. 4e, brown traces). Again, the reaction proceeded markedly faster than in the absence of nanoparticles, although somewhat slower than with Au; this discrepancy between equally sized gold and magnetite nanoparticles could be attributed to the higher surface density of azobenzene on Au.

We then investigated the effect of cycle duration on the conversion of **13**. In this series of experiments, a total of 60 min of ultraviolet irradiation of **13** was divided into 60 cycles of 1 min, 40 cycles of 1.5 min, and so on, down to 3 cycles of 20 min (each cycle separated by 1 min of visible light). We found a sharp peak in the plot of conversion versus cycle duration, with 20 three-minute cycles producing the fullest conversion (Fig. 4f). These results suggest that, within this period, (1) nanoparticle self-assembly and guest trapping proceeded to a considerable extent and (2) the majority of trapped molecules underwent dimerization. Interestingly, these results can be correlated with time-resolved studies of the self-assembly process, which revealed that ~3 min of ultraviolet irradiation were needed to observe the formation of densely packed nanoparticle aggregates (Supplementary Section 16) (given that this time scale is long compared to diffusion of small molecules allows us to speculate that the trapping process is predominantly thermodynamic in nature).

Finally, we hypothesized that the trapping in the dynamic nanoflasks can alter the chemical reactivity of the trapped species. For example, when ultraviolet-induced dimerization of **13** is attempted in non-deoxygenated solutions, it is outcompeted by rapid oxidative degradation to anthraquinone[45–47] (>95% oxidation with negligible dimerization over 60 min). We found, however, that capturing **13** within nanoflasks rendered it inert to the typically undesired photo-oxidation reaction: visible light-induced disassembly of nanoparticle aggregates exposed to 60 min of ultraviolet released a mixture of **13** and **14** with no detectable oxidation product. Furthermore, the nature of **14** depended on whether it was formed inside or outside the nanoflasks. On dimerization, **13** can form two isomers of **14**, indicated by *syn* and *anti* in Fig. 4d[48,49]. Dimerization in nanoparticle-free solutions yields almost exclusively the thermodynamic product *anti*-**14** (we observed less than 2% *syn*). In the presence of the nanoflasks, however, we observed as much as >80% of **14** as the *syn* isomer (Fig. 4g). We speculate that the high yield of the otherwise unstable isomer is due to the pre-organization[13] of **13** inside the nanoflasks via hydrogen-bonding interactions with *cis*-azobenzene before the dimerization takes place. Similarly, anthracenes **15** and **16** dimerized with increased kinetics in the presence of self-assembling 6 nm Au·**1** (Fig. 4h–j). Notably, the *syn*-to-*anti* ratio for the dimer of **15** was the same

irrespective of the presence of nanoparticles. This result can be explained by the similar dipole moments of the *syn*- and *anti*-dimers of **15** and by the lack of strong hydrogen-bonding ability of **15**. Similar to **13**, **16** dimerizing in solution afforded almost exclusively the thermodynamic *anti* product (Fig. 4j). In contrast, dimerization in the presence of nanoparticles resulted in an appreciable amount of the *syn* isomer (although less than in the case of **13**, ~35 and ~81%, respectively, a result that could be explained by the lack of preorganization-promoting hydrogen-bond interactions between the CN groups and the *cis*-azobenzene moieties). Overall, these results highlight the possibility of using the nanoflasks for altering stereoselectivities on demand.

Conclusions

We have described a novel class of synthetic confined environments—dynamically self-assembling nanoflasks—whose formation and disassembly are governed by irradiation with light of different wavelengths. The dimensions of these nanoflasks can be tuned by the diameters of the constituent nanoparticles as well as by the lengths of the ligands on their surfaces. The nanoflasks can trap various molecules from solution as they self-assemble. The trapping selectivity could be increased by functionalizing the nanoparticles with mixed monolayers comprising light-sensitive groups and ligands carrying specific recognition units. The trapped molecules can undergo chemical reactions with faster kinetics and with stereoselectivities different from those in bulk solution. Although similar effects could in principle be observed on planar surfaces, the high overall surface areas of small nanoparticles make it possible to carry out reactions on a large scale. We envision the application of the nanoflasks as nanoreactors, for example, for the polymerization of trapped monomers (with the lengths of the polymer chains determined by the dimensions of the nanoflasks), for enantioselective reactions (taking advantage of the chiral nanoflasks), as well as for preparing diverse classes of inorganic nanostructures.

Received 29 March 2015; accepted 5 October 2015; published online 23 November 2015

References

1. Poole, L. B., Karplus, P. A. & Claiborne, A. Protein sulfenic acids in redox signaling. *Annu. Rev. Pharmacol. Toxicol.* **44,** 325–347 (2004).
2. Tripp, B. C., Smith, K. & Ferry, J. G. Carbonic anhydrase: new insights for an ancient enzyme. *J. Biol. Chem.* **276,** 48615–48618 (2001).
3. Forman, H. J. & Fridovic, I. Superoxide dismutase: a comparison of rate constants. *Arch. Biochem. Biophys.* **158,** 396–400 (1973).
4. Hong, Y. J. & Tantillo, D. J. Consequences of conformational preorganization in sesquiterpene biosynthesis: theoretical studies on the formation of the bisabolene, curcumene, acoradiene, zizaene, cedrene, duprezianene, and sesquithuriferol sesquiterpenes. *J. Am. Chem. Soc.* **131,** 7999–8015 (2009).
5. Yasumoto, T. & Murata, M. Marine toxins. *Chem. Rev.* **93,** 1897–1909 (1993).
6. Nissen, P., Hansen, J., Ban, N., Moore, P. B. & Steitz, T. A. The structural basis of ribosome activity in peptide bond synthesis. *Science* **289,** 920–930 (2000).
7. Faivre, D. & Schuler, D. Magnetotactic bacteria and magnetosomes. *Chem. Rev.* **108,** 4875–4898 (2008).
8. Aizenberg, J., Tkachenko, A., Weiner, S., Addadi, L. & Hendler, G. Calcitic microlenses as part of the photoreceptor system in brittlestars. *Nature* **412,** 819–822 (2001).
9. Li, X. Y. & Liu, D. R. DNA-templated organic synthesis: nature's strategy for controlling chemical reactivity applied to synthetic molecules. *Angew. Chem. Int. Ed.* **43,** 4848–4870 (2004).
10. Kanan, M. W., Rozenman, M. M., Sakurai, K., Snyder, T. M. & Liu, D. R. Reaction discovery enabled by DNA-templated synthesis and *in vitro* selection. *Nature* **431,** 545–549 (2004).
11. Mal, P., Breiner, B., Rissanen, K. & Nitschke, J. R. White phosphorus is air-stable within a self-assembled tetrahedral capsule. *Science* **324,** 1697–1699 (2009).
12. Yoshizawa, M., Kusukawa, T., Fujita, M. & Yamaguchi, K. Ship-in-a-bottle synthesis of otherwise labile cyclic trimers of siloxanes in a self-assembled coordination cage. *J. Am. Chem. Soc.* **122,** 6311–6312 (2000).
13. Yoshizawa, M., Tamura, M. & Fujita, M. Diels–Alder in aqueous molecular hosts: unusual regioselectivity and efficient catalysis. *Science* **312,** 251–254 (2006).
14. Sastre, G. & Corma, A. The confinement effect in zeolites. *J. Mol. Catal. A* **305,** 3–7 (2009).
15. Chu, Y. Y., Han, B., Zheng, A. M. & Deng, F. Influence of acid strength and confinement effect on the ethylene dimerization reaction over solid acid catalysts: a theoretical calculation study. *J. Phys. Chem. C* **116,** 12687–12695 (2012).
16. Kundu, P. K., Olsen, G. L., Kiss, V. & Klajn, R. Nanoporous frameworks exhibiting multiple stimuli responsiveness. *Nature Commun.* **5,** 3588 (2014).
17. Wei, Y.-S. *et al.* Coordination templated [2+2+2] cyclotrimerization in a porous coordination framework. *Nature Commun.* **6,** 8348 (2015).
18. Fallah-Araghi, A. *et al.* Enhanced chemical synthesis at soft interfaces: a universal reaction–adsorption mechanism in microcompartments. *Phys. Rev. Lett.* **112,** 028301 (2014).
19. Yang, D. Y. *et al.* Enhanced transcription and translation in clay hydrogel and implications for early life evolution. *Sci. Rep.* **3,** 3165 (2013).
20. Komisarski, M., Osornio, Y. M., Siegel, J. S. & Landau, E. M. Tailored host–guest lipidic cubic phases: a protocell model exhibiting nucleic acid recognition. *Chem. Eur. J.* **19,** 1262–1267 (2013).
21. Crosby, J. *et al.* Stabilization and enhanced reactivity of actinorhodin polyketide synthase minimal complex in polymer–nucleotide coacervate droplets. *Chem. Commun.* **48,** 11832–11834 (2012).
22. Shevchenko, E. V., Talapin, D. V., Murray, C. B. & O'Brien, S. Structural characterization of self-assembled multifunctional binary nanoparticle superlattices. *J. Am. Chem. Soc.* **128,** 3620–3637 (2006).
23. Macfarlane, R. J. *et al.* Nanoparticle superlattice engineering with DNA. *Science* **334,** 204–208 (2011).
24. Sanchez-Iglesias, A. *et al.* Hydrophobic interactions modulate self-assembly of nanoparticles. *ACS Nano* **6,** 11059–11065 (2012).
25. Nykypanchuk, D., Maye, M. M., van der Lelie, D. & Gang, O. DNA-guided crystallization of colloidal nanoparticles. *Nature* **451,** 549–552 (2008).
26. Kalsin, A. M. *et al.* Electrostatic self-assembly of binary nanoparticle crystals with a diamond-like lattice. *Science* **312,** 420–424 (2006).
27. Klajn, R., Wesson, P. J., Bishop, K. J. M. & Grzybowski, B. A. Writing self-erasing images using metastable nanoparticle 'inks'. *Angew. Chem. Int. Ed.* **48,** 7035–7039 (2009).
28. Lee, J.-W. & Klajn, R. Dual-responsive nanoparticles that aggregate under the simultaneous action of light and CO_2. *Chem. Commun.* **51,** 2036–2039 (2015).
29. Das, S. *et al.* Dual-responsive nanoparticles and their self-assembly. *Adv. Mater.* **25,** 422–426 (2013).
30. Chovnik, O., Balgley, R., Goldman, J. R. & Klajn, R. Dynamically self-assembling carriers enable guiding of diamagnetic particles by weak magnets. *J. Am. Chem. Soc.* **134,** 19564–19567 (2012).
31. Manna, A. *et al.* Optimized photoisomerization on gold nanoparticles capped by unsymmetrical azobenzene disulfides. *Chem. Mater.* **15,** 20–28 (2003).
32. Klajn, R., Bishop, K. J. M. & Grzybowski, B. A. Light-controlled self-assembly of reversible and irreversible nanoparticle suprastructures. *Proc. Natl Acad. Sci. USA* **104,** 10305–10309 (2007).
33. Biedermann, F., Uzunova, V. D., Scherman, O. A., Nau, W. M. & De Simone, A. Release of high-energy water as an essential driving force for the high-affinity binding of cucurbit[*n*]urils. *J. Am. Chem. Soc.* **134,** 15318–15323 (2012).
34. Biedermann, F., Vendruscolo, M., Scherman, O. A., De Simone, A. & Nau, W. M. Cucurbit[8]uril and blue-box: high-energy water release overwhelms electrostatic interactions. *J. Am. Chem. Soc.* **135,** 14879–14888 (2013).
35. Biedermann, F., Nau, W. M. & Schneider, H.-J. The hydrophobic effect revisited—studies with supramolecular complexes imply high-energy water as a noncovalent driving force. *Angew. Chem. Int. Ed.* **53,** 11158–11171 (2014).
36. Grego, A., Muller, A. & Weinstock, I. A. Stepwise-resolved thermodynamics of hydrophobic self-assembly. *Angew. Chem. Int. Ed.* **52,** 8358–8362 (2013).
37. Heaven, M. W., Dass, A., White, P. S., Holt, K. M. & Murray, R. W. Crystal structure of the gold nanoparticle $N(C_8H_{17})_4Au_{25}(SCH_2CH_2Ph)_{18}$. *J. Am. Chem. Soc.* **130,** 3754–3755 (2008).
38. Zhu, M., Lanni, E., Garg, N., Bier, M. E. & Jin, R. Kinetically controlled, high-yield synthesis of Au_{25} clusters. *J. Am. Chem. Soc.* **130,** 1138–1139 (2008).
39. Kondo, M., Takemoto, M., Matsuda, T., Fukae, R. & Kawatsuki, N. Photoinduced change in mechanical properties of anthracene polymers containing flexible side chains. *Bull. Chem. Soc. Jpn* **83,** 1333–1337 (2010).
40. Xu, J. F., Chen, Y. Z., Wu, L. Z., Tung, C. H. & Yang, Q. Z. Dynamic covalent bond based on reversible photo 4+4 cycloaddition of anthracene for construction of double-dynamic polymers. *Org. Lett.* **15,** 6148–6151 (2013).
41. Bouas-Laurent, H., Castellan, A., Desvergne, J. P. & Lapouyade, R. Photodimerization of anthracenes in fluid solution: structural aspects. *Chem. Soc. Rev.* **29,** 43–55 (2000).
42. Jain, P. K., Huang, X. H., El-Sayed, I. H. & El-Sayed, M. A. Noble metals on the nanoscale: optical and photothermal properties and some applications in imaging, sensing, biology, and medicine. *Acc. Chem. Res.* **41,** 1578–1586 (2008).

43. Harris, N., Ford, M. J. & Cortie, M. B. Optimization of plasmonic heating by gold nanospheres and nanoshells. *J. Phys. Chem. B* **110,** 10701–10707 (2006).
44. Neumann, O. *et al*. Solar vapor generation enabled by nanoparticles. *ACS Nano* **7,** 42–49 (2013).
45. Fox, M. A. & Olive, S. Photo-oxidation of anthracene on atmospheric particulate matter. *Science* **205,** 582–583 (1979).
46. Alonso, R., Jimenez, M. C. & Miranda, M. A. Stereodifferentiation in the compartmentalized photooxidation of a protein-bound anthracene. *Org. Lett.* **13,** 3860–3863 (2011).
47. Alonso, R., Yamaji, M., Jimenez, M. C. & Miranda, M. A. Enhanced photostability of the anthracene chromophore in aqueous medium upon protein encapsulation. *J. Phys. Chem. B* **114,** 11363–11369 (2010).
48. Tung, C. H. & Guan, J. Q. Regioselectivity in the photocycloaddition of 9-substituted anthracenes incorporated within nafion membranes. *J. Org. Chem.* **63,** 5857–5862 (1998).
49. Arumugam, S., Vutukuri, D. R., Thayumanavan, S. & Ramamurthy, V. A styrene based water soluble polymer as a reaction medium for photodimerization of aromatic hydrocarbons in water. *J. Photochem. Photobiol. A* **185,** 168–171 (2007).

Acknowledgements

This work was supported by the European Research Council (grant no. 336080; R.K.), the NSF Division of Materials Research (grant no. 1309765; P.K.) and the American Chemical Society Petroleum Research Fund (grant no. 53062-ND6; P.K.). The authors thank R. Neumann and his group for the use of their gas chromatograph and T. Zdobinsky for technical assistance.

Author contributions

R.K. conceived the project. H.Z., T.U., M.S., K.K., D.M., P.K.K. and J.-W.L. performed the experiments and analysed the data. P.K. and S.S. performed the computer simulations. R.K. wrote the paper.

Additional information

Supplementary information is available in the online version of the paper. Reprints and permissions information is available online at www.nature.com/reprints. Correspondence and requests for materials should be addressed to R.K.

Competing financial interests

The authors declare no competing financial interests.